remote sensing

MDPI

Article

Lightning Detection Using GEO-KOMPSAT-2A/Advanced Meteorological Imager and Ground-Based Lightning Observation Sensor LINET Data

Seung-Hee Lee and Myoung-Seok Suh *

Department of Atmospheric Science, Kongju National University, 56 Gongjudaehak-ro, Gongju-si 32588, Republic of Korea; hjcall0122@smail.kongju.ac.kr
* Correspondence: sms416@kongju.ac.kr; Tel.: +82-41-850-8533

Abstract: In this study, GEO-KOMPSAT-2A/Advanced Meteorological Imager (GK2A/AMI) and Lightning NETwork (LINET) data were used for lightning detection. A total of 20 lightning cases from the summer of 2020–2021 were selected, with 14 cases for training and 6 for validation to develop lightning detection algorithms. Since these two datasets have different spatiotemporal resolutions, spatiotemporal matching was performed to use them together. To find the optimal lightning detection algorithm, we designed 25 experiments and selected the best experiment by evaluating the detection level. Although the best experiment had a high POD (>0.9) before post-processing, it also showed over-detection of lightning. To minimize the over-detection problem, statistical and Region-Growing post-processing methods were applied, improving the detection performance (FAR: −19.14~−24.32%; HSS: +76.92~+86.41%; Bias: −59.3~−66.9%). Also, a sensitivity analysis of the collocation criterion between the two datasets showed that the detection level improved when the spatial criterion was relaxed. These results suggest that detecting lightning in mid-latitude regions, including the Korean Peninsula, is possible by using GK2A/AMI data. However, reducing the variability in detection performance and the high FAR associated with anvil clouds and addressing the parallax problem of thunderstorms in mid-latitude regions are necessary to improve the detection performance.

Keywords: lightning detection; GK2A/AMI; collocation criteria; post-processing

check for updates

Citation: Lee, S.-H.; Suh, M.-S. Lightning Detection Using GEO-KOMPSAT-2A/Advanced Meteorological Imager and Ground-Based Lightning Observation Sensor LINET Data. *Remote Sens.* **2024**, *16*, 4243. https://doi.org/10.3390/rs16224243

Academic Editor: Yuriy Kuleshov

Received: 27 September 2024
Revised: 6 November 2024
Accepted: 12 November 2024
Published: 14 November 2024

Copyright: © 2024 by the authors. Licensee MDPI, Basel, Switzerland. This article is an open access article distributed under the terms and conditions of the Creative Commons Attribution (CC BY) license (https://creativecommons.org/licenses/by/4.0/).

1. Introduction

Lightning is a spark discharge between separated and accumulated negative and positive charges within a cloud as a tall cumulonimbus cloud develops or between the charges at the bottom of the cloud and the charges on the ground [1–3]. The Korean Peninsula, located on the continent's eastern edge, experiences an influx of warm and humid air from southerly or westerly winds associated with the East Asian monsoon during summer, leading to active deep convection [4–8]. Deep convection in a warm and humid environment causes hazardous weather phenomena such as thunderstorms and heavy rainfall [9]. Therefore, lightning occurs more frequently in the summer season on the Korean Peninsula than in other seasons, and the strong interannual and intraseasonal variability of the East Asian summer monsoon and the Northwestern Pacific High contributes to the significant spatiotemporal variability of lightning-inducing systems [10,11].

Recently, due to global warming, there has been a trend of an increasing frequency and intensity of lightning. Notably, the lightning frequency has increased in high-altitude regions that are sensitive to warming [12,13]. Additionally, Pérez-Invernón et al. [14] predicted future lightning occurrence frequencies under the RCP6.0 scenario. They found that by the 2090s, with a 1 K increase in temperature, the global lightning occurrence frequency is expected to increase by about 11%.

Lightning, when it occurs, not only causes casualties but can also ignite wildfires and damage the aviation and aerospace industries, making the detection and prediction of

lightning increasingly important [15–17]. Accordingly, domestically and internationally, research on the statistical characteristics, detection, and prediction of convective clouds or lightning is actively being conducted.

Studies on the statistical characteristics mainly focus on the spatiotemporal distribution and instability index using ground-based lightning detection data. Eom and Suh [11] confirmed that 75% of annual lightning strikes occurred during the summer using data from the Korea Meteorological Administration (KMA)'s Total Lightning Detection System (TLDS) from 2002 to 2006. Myoung and Suh [18] found that negative lightning strikes in the Korean Peninsula occur more frequently than positive ones, comprising about 92% of all lightning strikes, which are particularly pronounced in the summer. In addition, various studies from multiple countries have presented findings on the strong spatiotemporal variability of lightning [12,19–21]. Eom and Suh [22] and Sfîcă et al. [23] analyzed stability indices during lightning occurrences. They showed that lightning frequently occurs when the atmosphere is unstable, suggesting that instability indices can be used to detect lightning. Bang [24] found that heavy rainfall mainly accompanies summer lightning using Lightning NETwork(LINET) and S-band polarimetric radar data, with radar reflectivity exceeding 45 dBZ during these events.

Additionally, many studies have been conducted using satellites to detect and predict convective clouds and lightning. Baek et al. [25] analyzed the characteristics of convective systems, utilizing the difference between the infrared and water vapor channels of Geostationary Operational Environmental Satellite (GOES)-9. Machado et al. [26] detected lightning by deriving an exponential function for the relationship between lightning and brightness temperature differences using the difference between the infrared and water vapor channels of GOES-12 and lightning observation data from the Brazilian Lightning Location System (RINDAT). They also revealed that positive brightness temperature differences are associated with Overshooting Convective Cloud Tops (OTs). Lee et al. [27], using data from the Multi-Functional Transport Satellite (MTSAT)-1R and TLDS, showed that during the summer months (June to August) of 2006 to 2008, the frequency of lightning was highest when the infrared channel brightness temperature was approximately 215 K, and the difference between the water vapor channel and the infrared channel was around 0 K. Also, several studies were conducted to detect and track thunderstorms in Korea by introducing the Rapid Development Thunderstorm (RDT) algorithm, which monitors the lifecycle of convective clouds in Europe using satellite data. These studies aimed to enhance the monitoring capabilities of the lifecycle of convective clouds by adjusting regression coefficients to fit the characteristics of lightning occurrence systems on the Korean Peninsula; they primarily utilized data from geostationary satellites (Himawari-8 and GEO-KOMPSAT-2A/Advanced Meteorological Imager (GK2A/AMI)) that observe the East Asian region and numerical model data from the KMA [28,29]. In addition, studies have been conducted to detect OTs associated with strong updrafts using satellite data [30,31].

Recently, with the diversification of machine learning and deep learning technologies, studies utilizing these methods have also been conducted. Han et al. [32] detected Convective Initiation (CI) using various machine learning techniques and the visible and infrared channels of the Communication, Ocean, and Meteorological Satellite (COMS) as input variables. They compared the detection performance of each technique and found that Random Forest had the best accuracy, with an average of 91.7%. Cintineo et al. [33] detected intense convection using Convolutional Neural Networks (CNNs) and the visible and infrared channels of GOES-16 and satellite-derived lightning-related products as input data. The Critical Success Index (CSI) was approximately 0.6. Additionally, Cintineo et al. [34] detected lightning using U-Net, a different deep-learning CNN technique, and the CSI ranged from approximately 0.3 to 0.5. Cross et al. [35] trained and detected lightning images using CNN-based models such as DeepLabv3+ and SegNet and demonstrated an excellent accuracy of over 80% for most models. Lesejane et al. [36] classified Ground-Strike Points (GSPs) using Bayesian networks and K-means clustering, revealing that the K-means method achieved a higher accuracy.

Although various lightning studies have been conducted domestically and internationally, the detection and prediction levels still need to be improved, and research on lightning using satellites is very limited on the Korean Peninsula. Additionally, because the Korean Peninsula is located in the mid-latitudes, it is unsuitable for utilizing the Lightning Imaging Sensor (LIS) of the Tropical Rainfall Measuring Mission (TRMM), which observes between 35°N and 35°S. Additionally, the observation period of TRMM/LIS has limitations in monitoring lightning occurring at random times in detail [27]. In East Asia, the Geostationary Lightning Mapper (GLM) onboard GOES-16 is not operationally utilized [37,38]. Therefore, research on lightning detection and prediction using geostationary satellites is necessary.

Since 2019, South Korea has officially operated the GK2A/AMI, which observes the Korean Peninsula at 2 min intervals. Compared to COMS, GK2A has significantly improved performance, with an approximately seven times higher observation frequency and four times better spatial resolution for the Korean Peninsula. And, its number of channels has increased from 5 to 16 [39]. Geostationary satellites can continuously observe the same area, allowing for the monitoring of the physical characteristics of clouds according to the lifecycle and development process of convective clouds [8,40]. Therefore, by detecting lightning from geostationary meteorological satellites, we can obtain detailed spatiotemporal characteristics of lightning occurrences across the globe [41,42]. Therefore, this study evaluated the possibility of detecting lightning in the surrounding areas of the Korean Peninsula using GK2A/AMI data, which has superior spatiotemporal resolution and 16 channels.

To accomplish this, we used LINET data from KMA, which has recently been shown to have improved lightning detection performance. We developed a lightning detection regression formula and evaluated its performance using 20 cases from the summer months (June to August) of 2020 and 2021. Section 2 of this paper describes the data and cases used, the data preprocessing method, and the performance evaluation method, and Section 3 presents the lightning detection results in detail. Section 4 is the discussion of this study, and finally, Section 5 summarizes the study's results.

2. Materials and Methods

In this study, we used LINET and the GK2A/AMI data for 20 lightning cases between June and August in 2020 and 2021. LINET, introduced and operational since 2014, observes the lightning type, polarity, intensity, time of occurrence, and location using the Time of Arrival (TOA) method with signals in the Very Low Frequency (VLF)/Low Frequency (LF) and Very High Frequency (VHF) ranges [43]. This method is different from the Time of Group Arrival (TOGA) method used by the World-Wide Lightning Location Network (WWLLN) [44] and the Arrival Time Difference (ATD) method used by the Sferic Time and Ranging Network (STARNET) [45]. Currently, LINET observes lightning at 21 observatories across the Korean Peninsula (red dots in Figure 1), and the detection efficiency is over 95% across the Korean Peninsula and the adjacent seas [46]. GK2A observes every 10 min and has 16 channels [39]. In this study, the Brightness Temperature (BT) of the infrared (IR) 8, 11, 13, and 14 channels (6.3 μm, 8.7 μm, 10.5 μm, and 11.2 μm) were used, with the IR 8 used as the upper-level Water Vapor (WV) channel. The spatial resolution of all the channels used is 2 km. In this study, considering the observation efficiency of LINET, the analysis area was set as shown in the light blue area of Figure 1. The sources of the two datasets are the KMA and the National Meteorological Satellite Center (NMSC), respectively.

This study was conducted following the sequence shown in Figure 2. First, since LINET provides data on lightning occurrences at arbitrary times and locations, while GK2A provides spatiotemporally regular gridded data, spatiotemporal matching was necessary to use both datasets together. There is no established optimal spatiotemporal matching criterion between ground-based lightning detection sensor data and satellite data, so various criteria have been applied. For example, Lee et al. [27] set the threshold criteria to ±5 min and a radius of 5 km. Météo-France [47] used spatiotemporal matching criteria of −15 to +5 min and a radius of 35 km. In this study, we performed spatiotemporal

collocation using the method shown in Figure 3. Temporally, lightning that occurred within ±5 min of the satellite observation time was considered the same lightning event. Spatially, based on the nearest satellite pixel to the lightning occurrence point (the red pixel in Figure 3), the pixel with the lowest BT10.5 (BT of the 10.5 μm channel) within a 15 × 15-pixel area was defined as the convective pixel (ix, jy) that caused the lightning (the green pixel in Figure 3). This value was set to account for cases where lightning does not occur directly under the convective cell. Because the spatiotemporal collocation criteria are very important in lightning detection, we performed a simple sensitivity experiment on these criteria and the results are presented in Section 4.

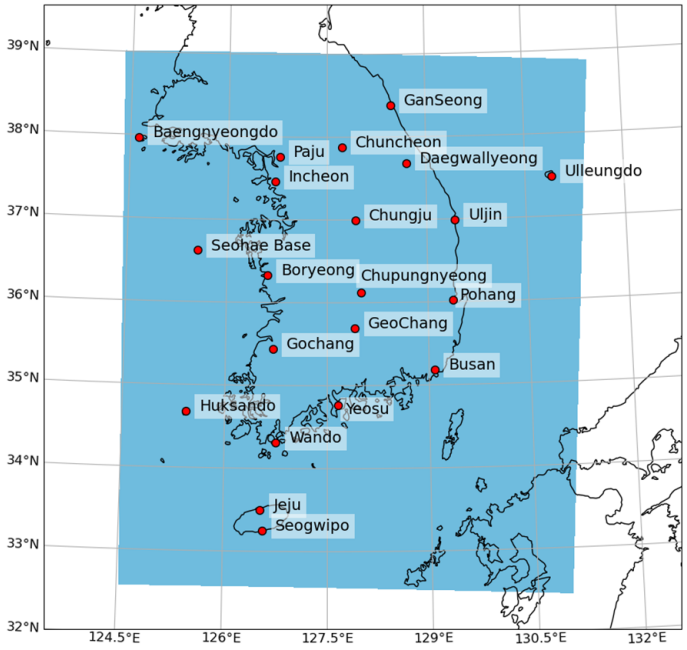


Figure 1. Analyzed area in this study (light blue area) and distribution of LINET sensors operated by the KMA (red dots).

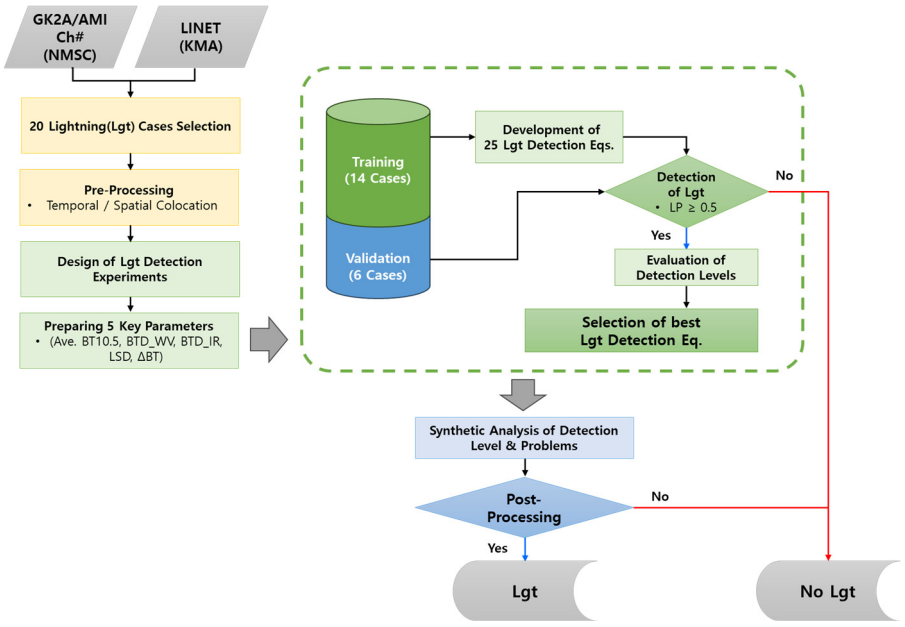


Figure 2. Flow chart of this study. "#" refers to a channel of GK2A/AMI.

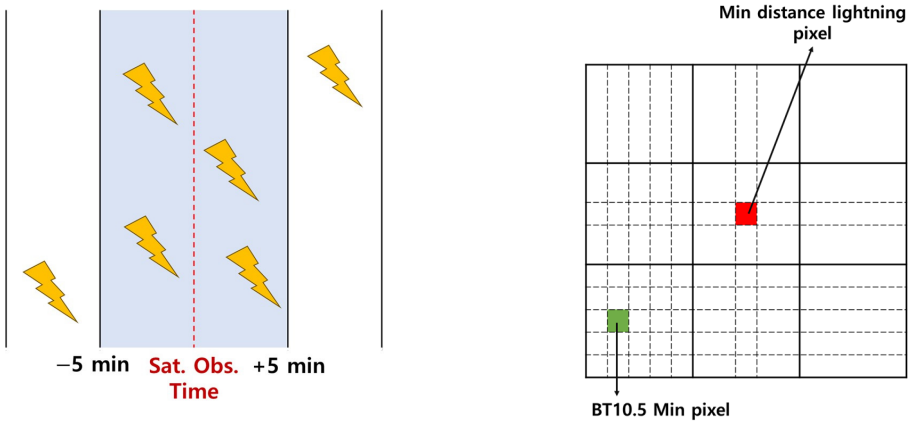


Figure 3. The method for temporal (**a**) and spatial (**b**) collocations of LINET data and GK2A/AMI data. In (**b**), the red pixel represents the nearest satellite pixel to the lightning occurrence point, and the green pixel indicates the pixel with the lowest BT10.5 within the 15 × 15 area surrounding the red pixel.

Although a convective pixel was selected through spatiotemporal collocation, deep convection that causes lightning has a horizontal scale that ranges from several kilometers to several tens of kilometers [48]. Therefore, this study used the BT as the average value of 3 × 3 pixels instead of a single pixel value (Equation (1)).

$$BT(Ch\#)_{Ave}(ix,jy) = \frac{1}{9}\sum_{k=ix-1}^{ix+1}\sum_{l=jy-1}^{jy+1} BT(Ch\#)(k,l) \quad (1)$$

Additionally, since lightning mainly occurs in clouds containing ice crystals, this study only used pixels where the $BT10.5_{Ave}$ was less than 250 K [49].

To leverage satellite data characteristics for strong convective cloud tops, we computed the brightness temperature difference (BTD) between channels. BTD_WV_{Ave} is the BTD between the upper WV channel (6.3 μm) and the atmospheric window channel (10.5 μm), which was calculated using Equation (2). This value indicates the development status of convective clouds, and shows a strong negative value in the early stage of convection, but as convection develops strongly, it has a value of 0 K [50]. BTD_IR_{Ave} is a variable for the cloud top phase (Equation (3)), utilizing the characteristic that the imaginary part of the refractive index of ice crystals is greater than that of water droplets in the 8.7 μm channel [51]. If the cloud is mainly composed of water droplets, it has a value of 0 or a negative value, but if it is composed of ice crystals, it has a positive value.

$$BTD_WV_{Ave}(ix,jy) = BT6.3_{Ave}(ix,jy) - BT10.5_{Ave}(ix,jy) \quad (2)$$

$$BTD_IR_{Ave}(ix,jy) = BT8.7_{Ave}(ix,jy) - BT11.2_{Ave}(ix,jy) \quad (3)$$

When convection becomes strong, the cloud surface becomes rough, and we estimated the intensity of convection by evaluating this roughness using the Local Standard Deviation (LSD) of $BT10.5_{Ave}$ (Equation (4)).

$$LSD_mbyn = \sqrt{\frac{\sum_{k=ix-\frac{m-1}{2}}^{ix+\frac{m-1}{2}}\sum_{l=jy-\frac{n-1}{2}}^{jy+\frac{n-1}{2}}\left(BT10.5(k,l) - \overline{BT}10.5_{ixjy}\right)^2}{m \times n}} \quad (4)$$

In Equation (4), $m \times n$ is the window size and $\overline{BT}10.5_{ixjy}$ is the average BT of the m×n area surrounding (ix, jy).

In addition, since the development or decline of convective clouds can be indicated by a temporal change (ΔBT_{Ave}) in BT, the change in BT was calculated and used as shown in Equation (5). At this time, the large temperature change due to cloud movement was excluded from the analysis.

$$\Delta BT_{Ave}(ix, jy, t) = BT10.5_{Ave}(ix, jy, t) - BT10.5_{Ave}(ix, jy, t - 10) \quad (5)$$

In this study, 20 lightning cases were selected to develop a lightning detection regression equation, which were divided into 14 training cases (T#) and 6 validation cases (V#). This is a total of 144 sets at 10 min intervals for 24 h a day, and the total dataset collected in this way for 20 days results in 144 sets/day × 20 days = 2880 sets. As shown in Table 1, the number of lightning occurrences per case varied greatly, from 705 to 21,079.

Table 1. Summary of lighting cases selected for training and validation.

Type	No.	Case	Count	No.	Case	Count
Training Cases	T1	22 August 2020	21,079	T8	7 August 2021	18,997
	T2	9 July 2020	19,482	T9	15 July 2021	13,467
	T3	29 July 2020	19,893	T10	16 July 2021	11,784
	T4	6 August 2020	9495	T11	2 August 2021	9964
	T5	11 August 2020	11,291	T12	18 August 2021	6367
	T6	26 August 2020	6211	T13	23 August 2021	11,812
	T7	23 July 2020	2832	T14	28 June 2021	3308
Validation Cases	V1	2 August 2020	8020	V4	22 June 2021	4346
	V2	6 July 2020	705	V5	10 July 2021	8992
	V3	12 June 2020	4331	V6	10 August 2021	9387

The regression equations for lightning detection were developed using five input variables (IV) related to the convective cloud characteristics calculated above. To account for various lightning-inducing systems and to identify as many combinations of satellite-observable factors as possible, 25 experiments (Exp#) based on combinations determined by the number of input variables (1 to 5) were performed (see Table 2). Considering that the relationship between the cloud top temperature and the lightning occurrence showed an exponential property in previous research [52], the regression equation for calculating the lightning probability (LP) used an exponential equation, as shown in Equation (6). a_n represents the regression coefficients. The dependent variable LP represents the ratio of the lightning count to the number of lightning pixels within the brightness temperature range of 190–250 K for 2 K intervals. In this study, a threshold of 0.5 was selected to indicate the absence of lightning, referencing Lee et al. [53] for the LP value. Because this threshold is very important, future research should conduct sensitivity tests on the threshold to optimize it.

$$LP = e^{a_1 IV_1 + a_2 IV_2 + a_3 IV_3 + a_4} \quad (6)$$

Table 2. Summary of lightning detection experiments by number of input variables.

Exp.	Input Variable(s)		Exp.	Input Variable(s)				
1	$BT10.5_{Ave}$		13	BTD_IR_{Ave}	LSD_3by3			
2	BTD_WV_{Ave}		14	BTD_IR_{Ave}	ΔBT_{Ave}			
3	BTD_IR_{Ave}		15	LSD_3by3	ΔBT_{Ave}			
4	LSD_3by3		16	$BT10.5_{Ave}$	BTD_WV_{Ave}	BTD_IR_{Ave}		
5	ΔBT_{Ave}		17	$BT10.5_{Ave}$	BTD_WV_{Ave}	LSD_3by3		
6	$BT10.5_{Ave}$	BTD_WV_{Ave}	18	$BT10.5_{Ave}$	BTD_IR_{Ave}	LSD_3by3		
7	$BT10.5_{Ave}$	BTD_IR_{Ave}	19	BTD_WV_{Ave}	BTD_IR_{Ave}	LSD_3by3		
8	$BT10.5_{Ave}$	LSD_3by3	20	$BT10.5_{Ave}$	BTD_WV_{Ave}	BTD_IR_{Ave}	LSD_3by3	
9	$BT10.5_{Ave}$	ΔBT_{Ave}	21	$BT10.5_{Ave}$	BTD_WV_{Ave}	BTD_IR_{Ave}	ΔBT_{Ave}	
10	BTD_WV_{Ave}	BTD_IR_{Ave}	22	$BT10.5_{Ave}$	BTD_WV_{Ave}	LSD_3by3	ΔBT_{Ave}	
11	BTD_WV_{Ave}	LSD_3by3	23	$BT10.5_{Ave}$	BTD_IR_{Ave}	LSD_3by3	ΔBT_{Ave}	
12	BTD_WV_{Ave}	ΔBT_{Ave}	24	BTD_WV_{Ave}	BTD_IR_{Ave}	LSD_3by3	ΔBT_{Ave}	
			25	$BT10.5_{Ave}$	BTD_WV_{Ave}	BTD_IR_{Ave}	LSD_3by3	ΔBT_{Ave}

Since lightning is a binary variable distinguished by whether it occurs, the detection performance was evaluated based on a contingency table (Figure 4). The performance evaluation indices used were Probability Of Detection (POD), False Alarm Ratio (FAR), Bias, Kuiper Skill Score (KSS), and Heidke Skill Score (HSS) (Equations (7)–(10)). According to Doswell et al. [54], HSS is superior to the Critical Success Index (CSI) in evaluating rare extreme events such as lightning or tornadoes. Therefore, this study used HSS for the evaluations.

$$POD = \frac{a}{OY} \text{ and } FAR = \frac{b}{DY} \tag{7}$$

$$Bias = \frac{DY}{OY} \tag{8}$$

$$KSS = POD - FAR \tag{9}$$

$$HSS = \frac{2 \times (a \times d - b \times c)}{(OY \times DN) + (DY \times ON)} \tag{10}$$

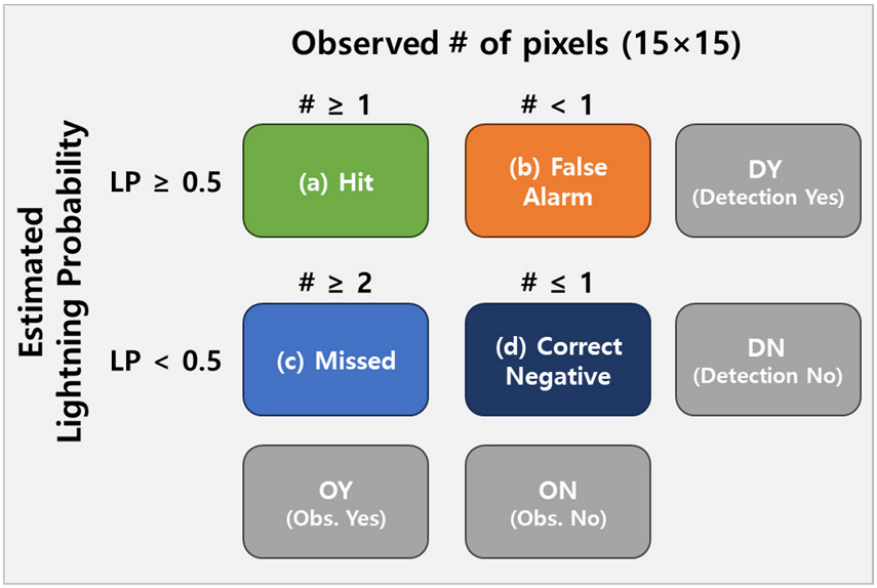


Figure 4. Contingency table for evaluation of lightning events. "#" represents the number of pixels.

After evaluating the detection performance in 25 experiments, we selected the best equation based on the POD, FAR, and HSS. The selected Exp had very high FAR and Bias values. Therefore, we performed two stages of post-processing to improve the lightning detection level. First, we aimed to remove clouds with a statistically higher non-occurrence rate than the lightning occurrence rate. To this end, we analyzed the density ratio of Hits and False Alarms for various combinations of five IVs (Equation (11)). Here, we post-processed clouds with a ratio of 50 or higher as clouds without lightning occurrence.

$$Ratio = \frac{False\ Alarm\ Count}{Hit\ Count} \tag{11}$$

The second step was the Region-Growing (RG) post-processing stage, which aimed to remove local false-detection pixels that remain even after statistical post-processing. The RG method is an image segmentation method that expands the region by checking the similarity of a 3 × 3 area based on a seed pixel. We counted the number of pixels in each cloud object, and clouds with fewer pixels than the threshold were removed. To determine the optimal pixel count threshold, we conducted sensitivity tests considering that the horizontal scale of meso-β is approximately 20 to 200 km.

3. Results

3.1. Results of Lightning Detection from 25 Experiments

In Figure 5 and Table 3, except for some Exps, the POD and FAR for all Exps were higher than 0.85. The long length of the boxes in the box plot indicates that the lightning detection performance varied from case to case. When comparing the detection performance between the training cases and validation cases, the variability in detection performance was greater in the validation cases. This is likely related to the fact that the lightning count was lower in the validation cases compared to the training cases, as shown in Table 1.

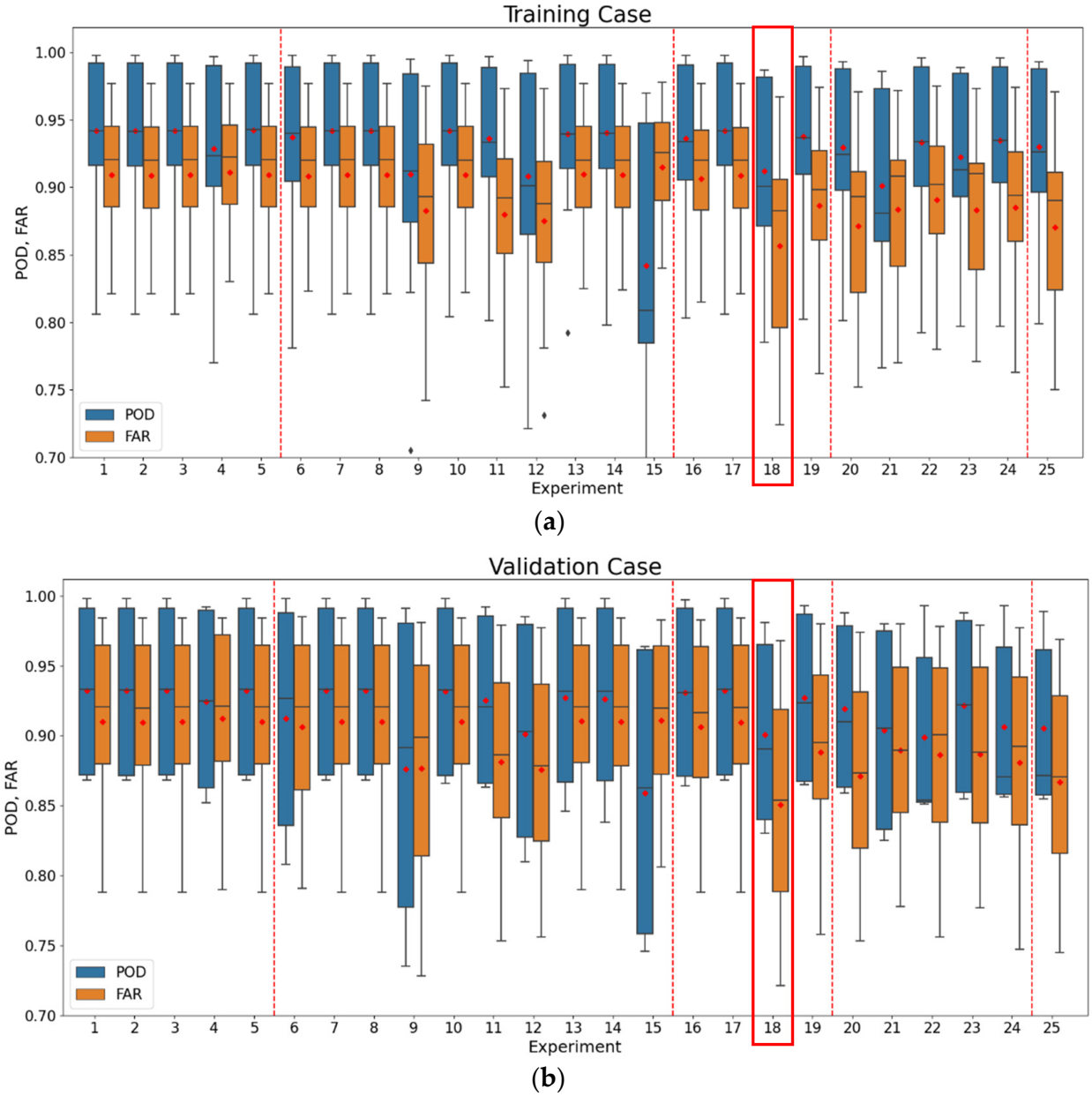


Figure 5. Box plots of lightning detection evaluation levels for the 25 Exps ((**a**) training and (**b**) validation cases). The red dots represent the average evaluation indices of the cases for each experiment. The red dashed lines divide the Exps based on the number of IVs. Red boxes show Exp 18, which had the best result among the 25 experiments.

Table 3. Skill scores for lightning detection in the training and validation cases in the 25 Exps. The bold text indicates the Exp with the highest detection performance.

Exp	Case	POD	FAR	HSS	Bias
1	Train	0.942	0.909	0.122	15.022
	Valid	0.932	0.910	0.129	23.323
2	Train	0.942	0.909	0.122	15.021
	Valid	0.932	0.909	0.130	23.214
3	Train	0.942	0.909	0.122	15.027
	Valid	0.932	0.910	0.128	23.375
4	Train	0.929	0.911	0.118	14.284
	Valid	0.925	0.912	0.127	22.741
5	Train	0.942	0.909	0.122	15.027
	Valid	0.932	0.910	0.128	23.375
6	Train	0.937	0.908	0.123	14.859
	Valid	0.912	0.906	0.134	22.114
7	Train	0.942	0.909	0.122	15.019
	Valid	0.923	0.901	0.129	22.317
8	Train	0.942	0.909	0.123	15.015
	Valid	0.923	0.901	0.129	22.315
9	Train	0.910	0.883	0.164	11.957
	Valid	0.873	0.868	0.176	16.756
10	Train	0.942	0.909	0.122	15.022
	Valid	0.932	0.910	0.129	22.323
11	Train	0.936	0.880	0.170	11.411
	Valid	0.925	0.881	0.177	15.055
12	Train	0.908	0.875	0.166	11.876
	Valid	0.901	0.878	0.171	14.539
13	Train	0.939	0.910	0.125	14.742
	Valid	0.927	0.910	0.130	22.843
14	Train	0.940	0.909	0.119	14.786
	Valid	0.926	0.910	0.131	22.685
15	Train	0.842	0.915	0.114	14.182
	Valid	0.859	0.911	0.128	20.615
16	Train	0.936	0.907	0.127	14.538
	Valid	0.931	0.906	0.135	21.313
17	Train	0.942	0.909	0.123	14.959
	Valid	0.932	0.910	0.132	22.216
18	**Train**	**0.912**	**0.857**	**0.206**	**9.329**
	Valid	**0.901**	**0.851**	**0.221**	**10.672**
19	Train	0.938	0.887	0.203	11.536
	Valid	0.927	0.888	0.219	16.725
20	Train	0.930	0.871	0.184	10.524
	Valid	0.919	0.871	0.193	12.961
21	Train	0.901	0.884	0.164	11.168
	Valid	0.904	0.889	0.163	16.406
22	Train	0.933	0.891	0.153	12.591
	Valid	0.899	0.886	0.167	14.969
23	Train	0.923	0.883	0.165	11.471
	Valid	0.921	0.887	0.167	16.263

Table 3. *Cont.*

Exp	Case	POD	FAR	HSS	Bias
24	Train	0.935	0.885	0.162	11.955
	Valid	0.906	0.881	0.177	14.109
25	Train	0.930	0.870	0.186	10.476
	Valid	0.905	0.867	0.199	11.417
Mean_IV_1	Train	0.939	0.909	0.121	14.876
	Valid	0.931	0.910	0.128	23.206
Mean_IV_2	Train	0.924	0.901	0.135	13.887
	Valid	0.910	0.898	0.143	20.156
Mean_IV_3	Train	0.932	0.890	0.165	12.591
	Valid	0.923	0.889	0.177	17.732
Mean_IV_4	Train	0.924	0.883	0.166	11.542
	Valid	0.910	0.883	0.173	14.942

In Table 3, the detection performance for each IV (Mean_IV_#) indicates an improvement in detection levels as the number of IVs utilized increased. When there was only one IV (Mean_IV_1: Exps 1–5), the detection levels were almost similar across Exps, and both the POD and FAR were higher than in the other Exps. This suggests that while using a single IV results in a high POD, it also leads to overfitting to each IV, causing the Bias to become very high. When there were two IVs (Mean_IV_2: Exps 6–15), the POD was generally higher than the FAR. However, in some Exps that include ΔBT_{Ave} (Exps 9 and 15), the detection performance was lower than that of the other Exps. This is likely because the ΔBT_{Ave} changes differently during the formation and dissipation phases of clouds that cause lightning. When there were three IVs (Mean_IV_3: Exps 16–19), two Exps (Exps 18 and 19) showed better detection than the other experiments. These Exps included BTD_IR_{Ave} and LSD_3by3, demonstrating that combining cloud top phase and roughness with other variables more effectively detects lightning.

To select the optimal regression formula among the 25 Exps, we comprehensively considered the POD, FAR, KSS, Bias, HSS, and the variability in lightning detection performance across the cases (the length of the boxes and whiskers in Figure 5). As shown in Figure 5 and Table 3, Exp 18 (Equation (12)), which used $BT10.5_{Ave}$, BTD_IR_{Ave}, and LSD_3by3, had the highest evaluation metrics. The HSS was above 0.2 in the training and validation cases, and the Bias was 9.329 in the training and 10.672 in the validation cases. This Exp demonstrated superior performance in lightning detection because most clouds that induce lightning develop thickly due to vigorous convective activity. In other words, the high and rough cloud tops resulting from active convection are detected by $BT10.5_{Ave}$, LSD_3by3, and BTD_IR_{Ave}. Therefore, this study selected Exp 18 as the best lightning detection regressor.

However, based on Figure 5 and Table 3, Exp 18 had a high FAR in both the training and validation cases. In particular, the HSS was low and there was an over-detection issue, with the Bias ranging from 9 to 10. Even if we take into account that LINET is optimized for cloud-to-ground (CG) lightning detection, which means that Intra-Cloud (IC) and Cloud-to-Cloud (CC) lightning detection rate is very low, having a Bias of 9 or more indicates a very high level of over-detection, which needs to be improved.

$$LP = e^{-0.08BT10.5_{Ave} - 1.05BTD_IR_{Ave} + 0.26LSD_3by3 + 18.61} \quad (12)$$

Figure 6a,b shows sample images of the BT10.5, lightning distribution, and lightning detection results from Exp 18 on 6 July, 2020, at 03:20 UTC. In this case, the lightning was triggered by a low-pressure system accompanying a stationary front, with only 26 lightning strikes at the selected time. Figure 6c,d shows images from 11 August 2020 at 05:30 UTC, where the lightning was caused by atmospheric instability due to the advection of warm,

humid air in the lower levels and cold, dry air in the upper levels, resulting in 103 lightning strikes at the selected time. Comparing the lightning detection results (Figure 6a,c) with the lightning strike locations (yellow markers in Figure 6a,c), the lightning strikes were strongly detected, but the red areas were widely distributed. These areas mainly corresponded to anvil clouds extending around convective cells or upper-level clouds with a low BT. Therefore, this study designed statistical and RG post-processing methods to improve the detection performance.

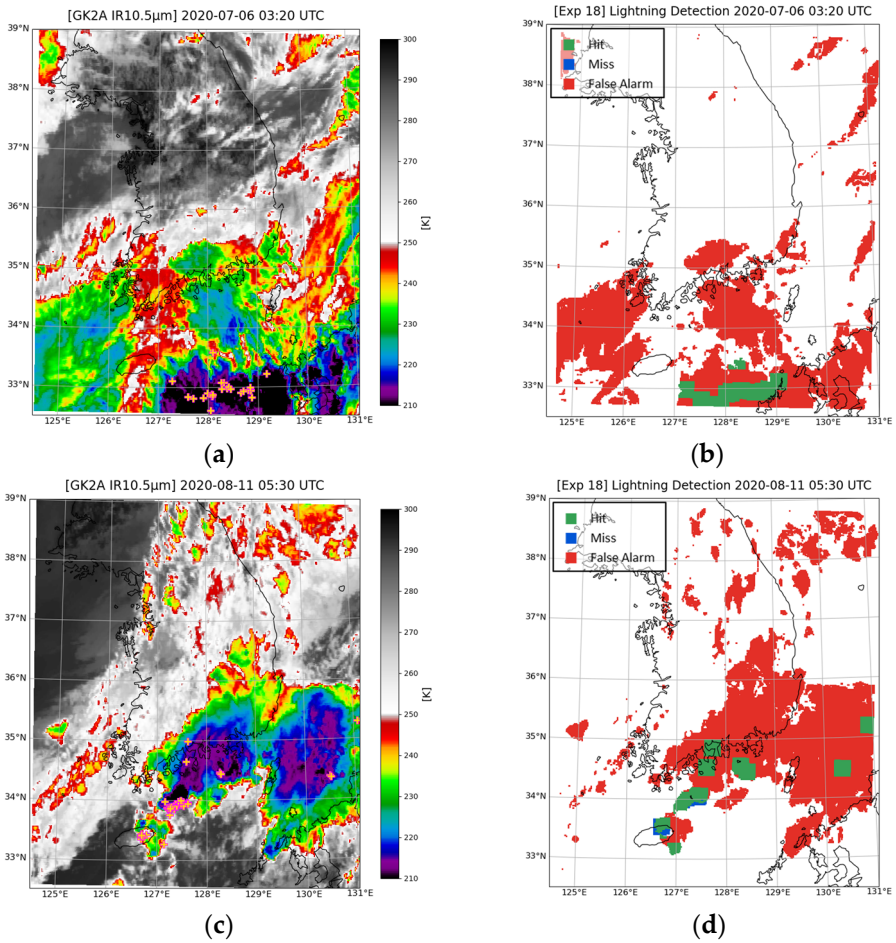


Figure 6. Sample images of (**a**,**c**) BT10.5 distribution with lightning occurrence points (yellow cross markers) and (**b**,**d**) lightning detection results from Exp 18. (**a**,**b**) There were fewer lightning occurrences at 03:20 UTC on 6 July 2020. (**c**,**d**) Intense lightning occurrences at 05:30 UTC on 11 August 2020.

3.2. Post-Processing for Improving Detection Performance

3.2.1. Statistical Post-Processing for False-Detection Pixels

To improve the problem of severe over-detection, we calculated the *Ratio*, representing the distribution of Hit pixels to False Alarm pixels. Among the various *Ratio* distributions, we aimed to statistically remove false-detection pixels using the distribution that prominently showed the characteristics of over-detection.

In Figure 7, the redder the *Ratio* distribution, the higher the *Ratio* of false detection. The pink region is where Equation (11) has a zero denominator and a non-zero numerator (Hit count = 0; False Alarm count $\neq$ 0). Most false-detection pixels were concentrated where the BTD_WV was approximately -6 K or lower, and as the negative BTD_WV increased, the LSD_5by5 of the false-detection pixels also increased. This suggests that the main causes of false detections are convective clouds with high roughness in their early development, cloud edges, or anvil clouds with low roughness at the cloud top.

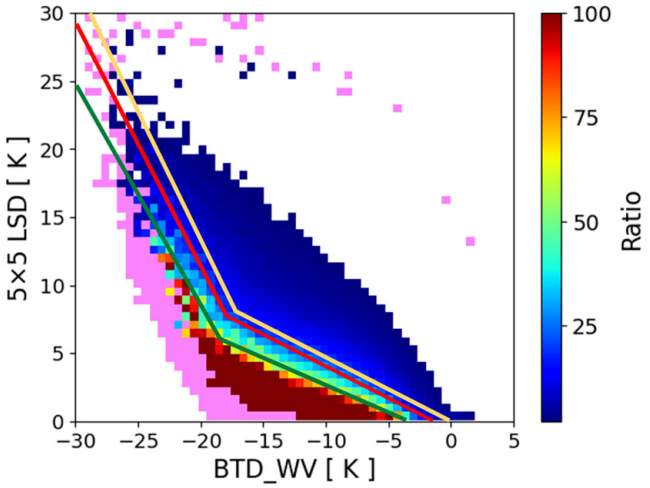


Figure 7. Distribution of the *Ratio* applied in statistical post-processing for Exp 18 (*Ratio*: the ratio of Hits to False Alarms, with the pink area representing regions where the Hit count = 0 and False Alarm count $\neq$ 0). The red line represents Test 9, and the green and orange lines represent Tests 7 and 10, respectively.

This study conducted sensitivity tests for Exp 18 to remove the clouds that caused false detections. The Test #s in Figure 8 represent the areas below the straight lines in Figure 7, which are indicated by the green, orange, and red lines. The sensitivity was analyzed by changing the slopes of these lines.

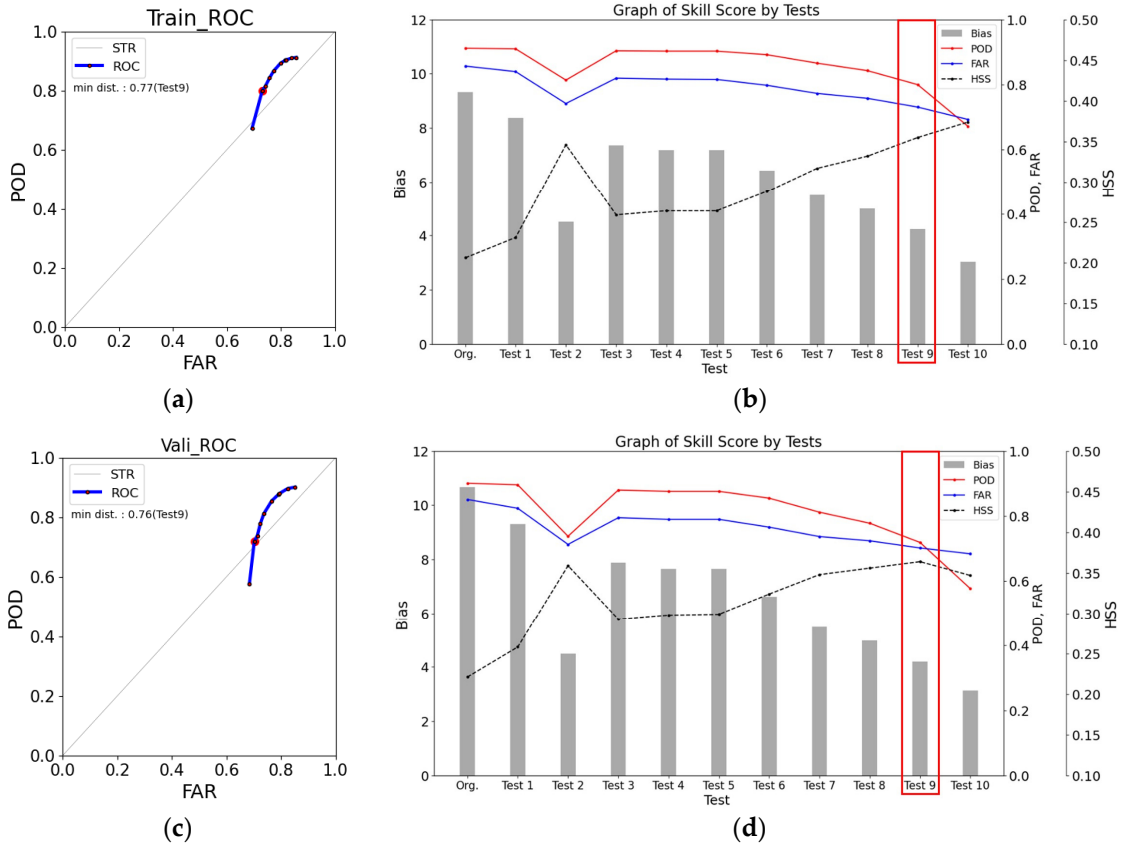


Figure 8. Results of sensitivity test for statistical post-processing of Exp 18 ((**a**,**b**): training cases; (**c**,**d**): validation cases). Test # refers to the tests based on the area below the line removed in Figure 7. The red box indicates the test with the best results from the sensitivity tests.

As a result of the sensitivity test, for Exp 18 (Figure 8), it was shown that applying Test 9 resulted in the best detection performance. The post-processing area for Test 9 is below the red line in Figure 7. As a result of the post-processing, the decrease in FAR was greater than that for the POD, and the HSS improved by approximately twofold. In particular, the Bias improved by more than threefold. This is also shown in the post-processed lightning detection images (Figure 9), where many areas of anvil clouds or immature clouds were removed.

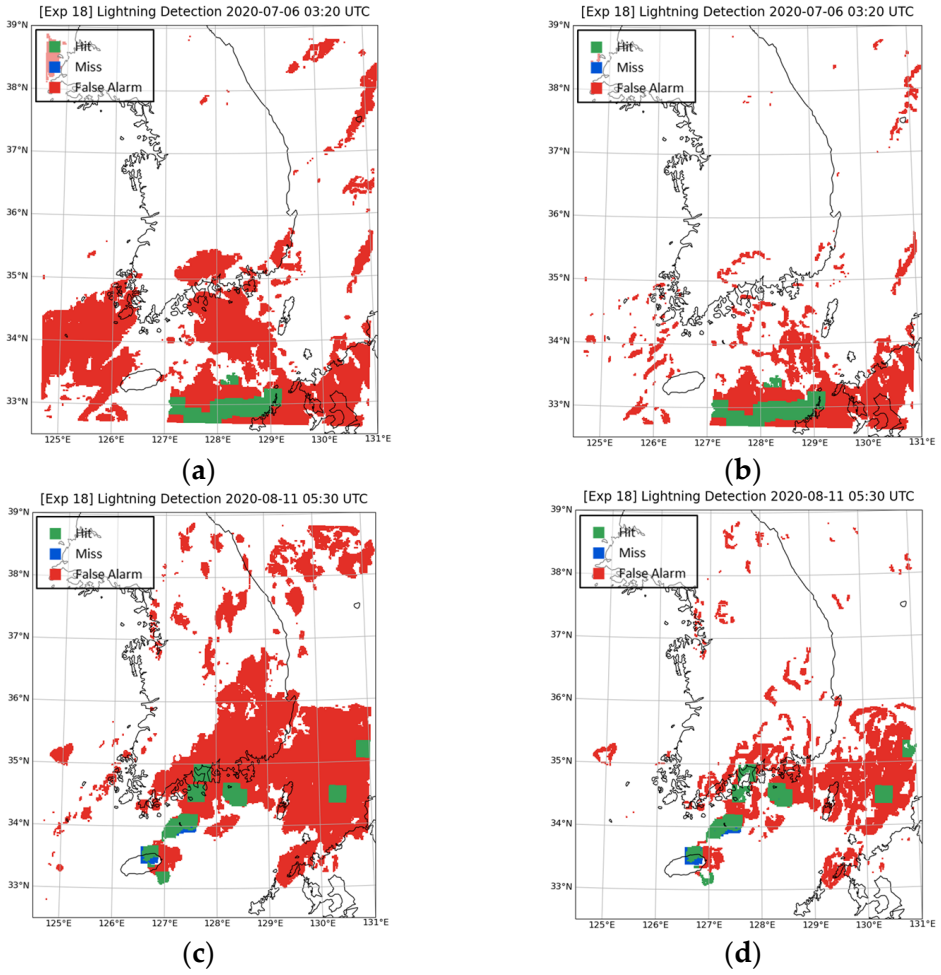


Figure 9. Sample images of lightning detection results before (**a**,**c**) and after (**b**,**d**) applying statistical post-processing.

3.2.2. Post-Processing Using Region-Growing Method

After statistical post-processing, the FAR and Bias were greatly improved, but the problem of false detection of small cloud cells still remained. Therefore, we aimed to remove small cloud cells using the RG method. From the results of the sensitivity test for the threshold pixels (Ref_pixel), Exp 18 showed the best performance when the Ref_pixel was 90, based on both the HSS and Bias (Figure 10). Considering that the resolution of the IR channels of GK2A/AMI is 4 km^2, this value corresponds to an area of 360 km^2. Since the minimum horizontal scale of the meso-β scale is about 20 km, with an area of approximately 314 km^2, this threshold corresponds to the smaller scale systems within the meso-β scale [55]. Although the improvement was less than that with the statistical post-processing, the Bias decreased to below 3.8. When comparing the distribution before and after applying RG (Figure 11), we can see that the small clouds causing the false detections were removed.

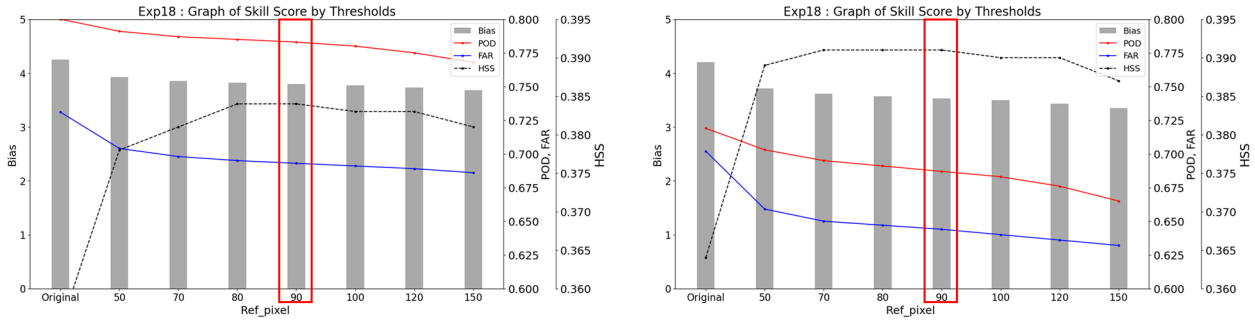


Figure 10. Results of the RG post-processing sensitivity test for the (**a**) training cases and (**b**) validation cases. The red box indicates that the Skill score for the threshold pixel (Ref_pixel) was 90, representing the final applied threshold value.

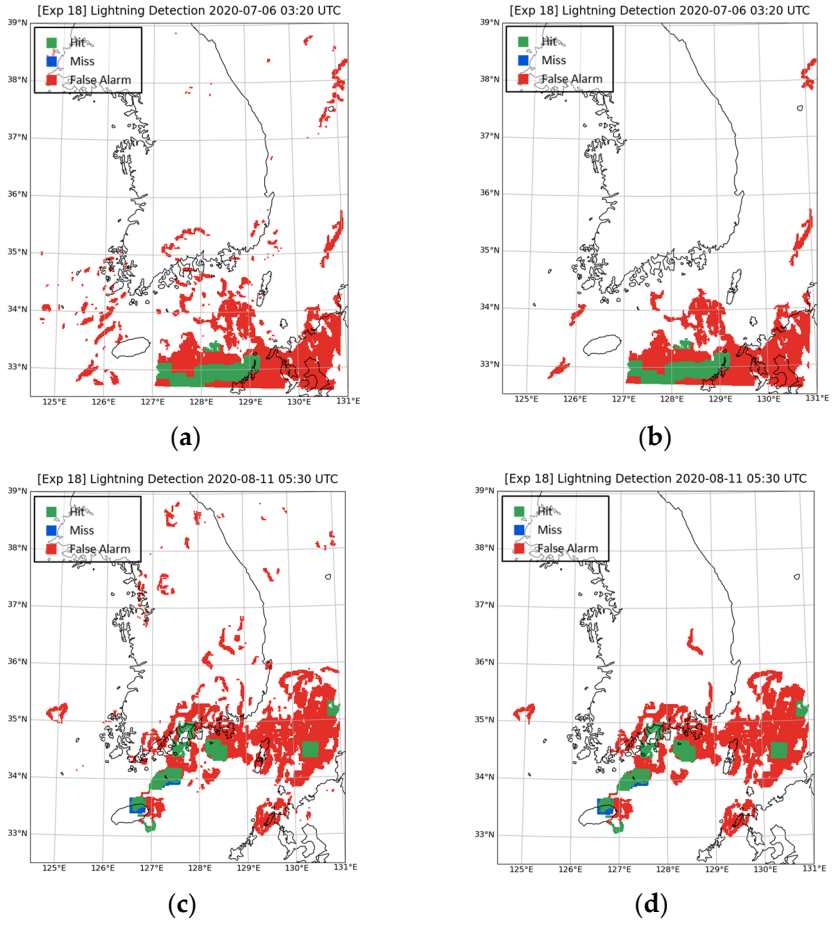


Figure 11. Sample images of lightning detection (**a**,**c**) before and (**b**,**d**) after applying RG post-processing with Ref_pixel = 90.

3.2.3. Comparison of Before and After Post-Processing Results

As a result of conducting statistical post-processing and RG post-processing, Table 4 shows that the POD ranged from 0.687 to 0.783, and the FAR ranged from 0.644 to 0.693. The HSS almost doubled, and the Bias was reduced by more than threefold. Considering that LINET has a very low detection rate for IC lightning, these results demonstrate the potential to detect lightning using GK2A/AMI. However, for operational use, it is necessary to address the issue of the relatively high FAR caused by thick anvil clouds or cloud edges. For example, developing a lightning detection algorithm that comprehensively considers

various systems that induce lightning is required. Moreover, considering other GK2A channels or supplementary outputs, such as atmospheric stability indices, as well as radar's Hybrid Surface Rainfall (HSR), is necessary.

Table 4. Results of lightning detection performance before and after the two-stage post-processing.

Exp.	Case		POD	FAR	HSS	Bias
18	Train	Before	0.912	0.857	0.206	9.329
		After (CR * [%])	0.783 (−14.14)	0.693 (−19.14)	0.384 (+86.41)	3.797 (−59.3)
	Valid	Before	0.901	0.851	0.221	10.672
		After (CR [%])	0.687 (−23.75)	0.644 (−24.32)	0.391 (+76.92)	3.532 (−66.9)

* Change Rate (CR) in each skill score before and after post-processing.

4. Discussion

This study analyzed the possibility of detecting lightning using South Korea's geostationary weather satellite GK2A/AMI. After detecting lightning using Exp 18, statistical and RG post-processing were applied, resulting in a POD of 0.687–0.783, FAR of 0.644–0.693, HSS of 0.384–0.391, and Bias of 3.532–3.797. This suggests the possibility of detecting lightning in areas such as the sea or high mountain regions, where ground-based lightning detection is not feasible using GK2A/AMI. However, there are issues where the detection performance varied by case, particularly with the Bias which was higher than 3.0.

It was anticipated that the lower performance in validation cases might be due to a lower frequency of lightning. To verify this, we analyzed the detection performance of Exp 18 for cases with a high lightning occurrence (High; V1, 5, and 6) and low lightning occurrence (Low; V2, 3, and 4) among the validation cases (Table 5). The results showed that cases with a higher lightning frequency yielded better evaluation indices. This indicates a limitation of the lightning detection algorithm in this study, as the detection performance decreased when the lightning occurrence was low. To address this, further analysis is needed on clouds with a low lightning occurrence, and it is essential to consider cases with a low lightning frequency when building training data.

Table 5. Detection performance of Exp 18 for validation cases with a high lightning occurrence (High; V1, 5, and 6) and low lightning occurrence (Low; V2, 3, and 4).

Exp	Case	POD	FAR	HSS	Bias
18	High	0.887	0.868	0.205	6.694
	Low	0.915	0.922	0.122	13.701

We applied statistical and RG post-processing to solve the severe false-detection and over-detection issues during the lightning detection process. Through this post-processing, the issues of false detection and over-detection were partially mitigated. However, there was an issue where both the POD and FAR decreased similarly, so it is necessary to discuss whether the post-processing applied in this study was effective. Statistical post-processing largely depends on the data used. Since our study only utilized 14 training cases, optimizing the thresholds used in the statistical post-processing with a more diverse set of cases is necessary for broader applicability. Also, in the RG post-processing, it was assumed that lightning does not occur in convective clouds smaller than 360 km^2. However, because lightning can occur even in cumulonimbus clouds smaller than the meso-β scale, it is essential to optimize the convective cloud size thresholds through research on various lightning-inducing systems. Additionally, the fact that the sharp decline in POD remained indicates the need for more sophisticated post-processing to address clouds that do not produce lightning.

This study performed spatiotemporal matching (Figure 3) to utilize satellite and lightning data together. The temporal and spatial criteria were set to ±5 min, based on the satellite observation time, and 15 × 15 pixels around the nearest lightning occurrence, respectively. However, the maximum charge separation area varies depending on factors such as the convective system's updraft speed, the differences in the occurrence region, the type of convective system (warm type or cold type), and the liquid water content within the cloud. Combined with the different ground conditions beneath the convective system, these lead to variations in the time, location, intensity, and polarity of lightning [56–58]. Therefore, a simple sensitivity experiment was conducted in this study to examine the impact of differences in spatiotemporal collocation on lightning detection.

Table 6 presents the experimental results after applying the same post-processing, with the temporal and spatial collocation criteria expanded to ±7 min and a 21 × 21-pixel area, respectively. Compared to the post-processing results with the original criteria, expanding the spatiotemporal criteria improved the lightning detection performance in most experiments. The FAR improved by 3.40–7.58%, and the HSS and Bias improved by up to 16.9% and 37.6%, respectively. Additionally, the sensitivity of lightning detection was more responsive to the spatial expansion, with the FAR reduction rate being approximately twice that of the POD reduction rate in both the training and validation cases. These results suggest that the spatiotemporal collocation criteria of the two datasets influence the lightning detection performance using GK2A/AMI data. Therefore, research on the spatiotemporal distribution characteristics between convection and lightning occurrence is necessary to achieve optimal spatiotemporal collocation.

Table 6. Results of post-processing for Exp 18 before and after changing the spatiotemporal collocation criteria. Bold text indicates values before changing the spatiotemporal collocation criteria.

Exp.	Case	Collocation Threshold	POD	FAR	HSS	Bias
18	Train (CR [%])	**±5 min, 15 × 15**	**0.783**	**0.693**	**0.384**	**3.797**
		±7 min, 15 × 15	0.757 (−3.32)	0.669 (−3.46)	0.399 (+3.91)	3.330 (−12.3)
		±5 min, 21 × 21	0.746 (−4.73)	0.613 (−11.54)	0.440 (+14.58)	2.751 (−27.55)
		±7 min, 21 × 21	0.720 (−8.05)	0.588 (−15.15)	0.449 (+16.93)	2.456 (−35.32)
	Valid (CR [%])	**±5 min, 15 × 15**	**0.687**	**0.644**	**0.391**	**3.532**
		±7 min, 15 × 15	0.657 (−4.37)	0.620 (−3.73)	0.397 (+1.53)	3.050 (−13.65)
		±5 min, 21 × 21	0.654 (−4.80)	0.558 (−13.35)	0.436 (+11.51)	2.485 (−29.64)
		±7 min, 21 × 21	0.624 (−9.17)	0.534 (−17.08)	0.437 (+11.76)	2.204 (−37.60)

Change Rate (CR) in each skill score before and after post-processing.

Lightning occurs more frequently over land than over the sea, and in the case of the Korean Peninsula, it is notably less common along the east coast and nearby regions [11,24]. Therefore, additional post-processing could be possible using the climatological distribution of lightning occurrences. Furthermore, Solimine et al. [59] suggested that while there is not always a linear relationship between lightning and heavy rainfall, using lightning data can enhance the estimation of convective rainfall rates. Consequently, incorporating radar HSR or reflectivity data and even radial velocity could improve lightning detection algorithms.

LINET's current lightning detection performance is about 95% [43]. However, LINET appears to have a low detection rate for Intra-Cloud (IC) and Cloud-to-Cloud (CC) lightning.

According to Medici et al. [60], IC and CC lightning occur more than four times as frequently as Cloud-to-Ground (CG) lightning. As shown in Figure 12, which shows the lightning detection rate for the summer of 2020–2021 on the Korean Peninsula, LINET's IC and CC lightning detection rate was very low. Considering the low detection rate of LINET for IC and CC lightning (Figure 12), which account for about 80% of lightning strikes, the actual performance of the lightning detection algorithm developed in this study can be considered not low.

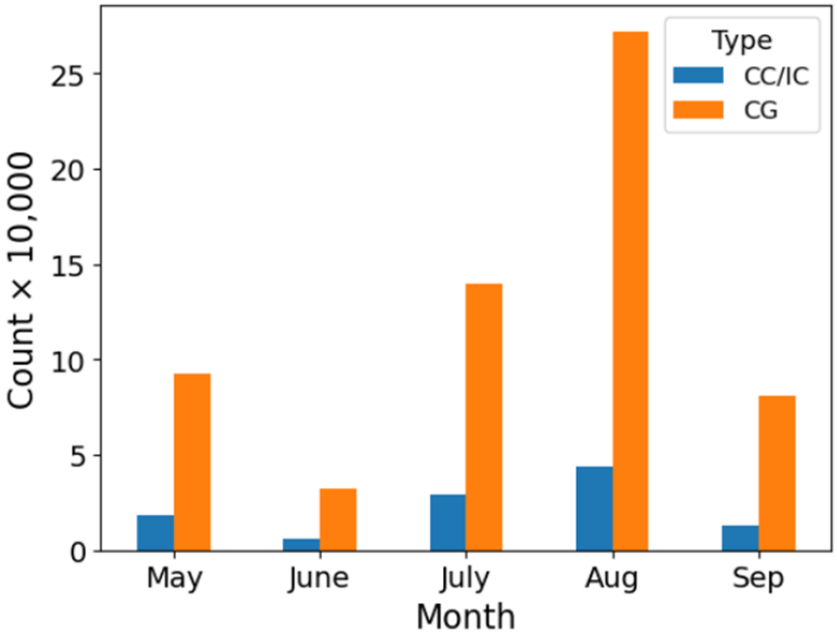


Figure 12. Monthly distribution of cloud-to-cloud (CC)/intracloud (IC) and cloud-to-ground (CG) lightning occurrences in the Korean Peninsula from May to September 2020–2021, as detected by LINET.

Also, when GK2A/AMI detects convective clouds that develop in mid-latitude regions such as the Korean Peninsula, the parallax issue causes positional errors in pixels, which likely affects the lightning detection accuracy when using GK2A/AMI [43,61]. Therefore, to improve lightning detection accuracy using geostationary satellite data, it is necessary to correct parallax errors and enhance ground-based lightning detection accuracy. In addition, in order to systematically construct a lightning database for East Asia or the whole world, it is necessary to use various lightning detection sensors, such as LIS/TRMM [62,63], GLM/GOES-# [64], and Lightning Mapping Imager (LMI)/FY-4A [65].

5. Conclusions

This study investigated the possibility of detecting lightning in the Korean Peninsula region using GK2A/AMI and LINET data. To this end, 20 lightning cases that occurred during the summer months (June–August) of 2020–2021 were selected. Since GK2A/AMI and LINET have different observation intervals and resolutions, a spatiotemporal collocation was performed to use the two datasets together. Temporally, lightning that occurred within ±5 min of the satellite observation time was defined as occurring at the same time. Spatially, the pixel with the lowest BT10.5 within a 15 × 15 area centered on the nearest satellite pixel to the lightning strike was defined as the convective pixel that caused the lightning. We divided the 20 selected cases into 14 training cases and 6 validation cases to develop the lightning detection regression equations. These equations were derived using exponential regression.

To select the optimal lightning detection regression equation, we utilized five IVs related to convective clouds ($BT10.5_{Ave}$, BTD_WV_{Ave}, BTD_IR_{Ave}, LSD_3by3, and ΔBT_{Ave})

and derived 25 lightning detection regression equations (Exps 1–25) using different numbers and combinations of IVs. The lightning detection results using Exps 1–25 showed that the lightning detection performance varied from case to case. Additionally, there were differences in detection performance depending on the number and combination of IVs. Considering the average and variability of the evaluation metrics for all regression equations, Exp 18, which used $BT10.5_{Ave}$, BTD_IR_{Ave}, and LSD_3by3, showed the best detection performance. Therefore, Exp 18 was selected as the optimal experiment because it used input variables that represent the characteristics of the upper part of convective clouds. For the lightning detection in Exp 18, the POD was higher than 0.9. However, the FAR was also higher than 0.85, and there was a severe over-detection problem with a Bias greater than 9, even though LINET's IC lightning detection rate is low.

To improve the over-detection problem, we aimed to statistically remove false-detection pixels by analyzing their characteristics. Therefore, we calculated and analyzed the ratio of the Hit count to False Alarm count, referred to as the *Ratio*. Among the various false-detection *Ratio* distributions, the *Ratio* was the highest in the distributions of BTD_WV, which indicates the development stage of clouds, and LSD_5by5, which represents the roughness of the cloud top. Analyzing the distribution of these *Ratio*s revealed that the false detections primarily occurred in immature convective cells, anvil clouds, relatively thick upper-level clouds, and cloud edges. Utilizing these characteristics for post-processing notably decreased the FAR. In particular, the Bias decreased by more than threefold, reducing the over-detection rate.

Despite applying statistical post-processing, false detections still occurred in the lightning detection result images, particularly in immature convective cells and cloud edges. Therefore, using the RG method, this study aimed to remove cells smaller than the meso-β scale, which is the size of mesoscale convective systems. Sensitivity experiments on the mesoscale convective cell criteria showed that when the number of cloud cell pixels was 90 (90×4 km^2 = 360 km^2), the best HSS and Bias were achieved.

After applying two-stage post-processing, the POD was 0.68–0.78, the FAR was 0.69–0.64, the HSS was 0.38, and the Bias was 3.5 for both the training and validation cases. Although the two-stage post-processing improved the lightning detection performance, improvements in the FAR and variability in detection performance across cases are necessary for operational use. This would enable the use of satellite data such as GK2A/AMI for lightning detection. Also, as discussed, it is necessary to improve the optimal distance between the convective core and lightning occurrence points, address the parallax issue in cumulonimbus clouds with high cloud tops in mid-latitude regions, and enhance the accuracy of LINET.

Author Contributions: Conceptualization, M.-S.S.; methodology, M.-S.S. and S.-H.L.; software, S.-H.L.; validation, S.-H.L.; formal analysis, S.-H.L. and M.-S.S.; investigation, S.-H.L.; resources, M.-S.S.; data curation, S.-H.L.; writing—original draft preparation, S.-H.L.; writing—review and editing, M.-S.S.; visualization, S.-H.L.; supervision, M.-S.S.; project administration, M.-S.S.; funding acquisition, M.-S.S. All authors have read and agreed to the published version of the manuscript.

Funding: This research was supported by the Korea Meteorological Administration Research and Development Program under Grant RS-2023-00239653 and the Specialized University Program for Confluence Analysis of Weather and Climate Data of the Korea Meteorological Institute (KMI) funded by the Korean government (KMA).

Data Availability Statement: Data from GK2A/AMI are freely available to registered users on the NMSC/KMA web portal: https://datasvc.nmsc.kma.go.kr/datasvc/html/main/main.do?lang=en (accessed on 23 August 2023). The LINET data are available from the KMA API Hub (https://apihub.kma.go.kr/; accessed on 23 August 2023).

Acknowledgments: We are grateful to the KMA and NMSC/KMA for providing vast amounts of lightning and satellite data.

Conflicts of Interest: The authors declare no conflicts of interest.

References

1. Mäkelä, A. Comparison between Lightning Data and Cloud Top Temperatures in Finland. In Proceedings of the 2006 EUMETSAT Meteorological Satellite Conference, Helsinki, Finland, 12–16 June 2006.
2. Korean Meteorological Society. *Easy-to-Understand Atmospheric Science*; Sigmapress: Seoul, Republic of Korea, 2020; p. 247.
3. NOAA National Severe Storms Laboratory Lightning Basics. Available online: https://www.nssl.noaa.gov/education/svrwx101/lightning/ (accessed on 5 July 2024).
4. Lee, D.-K.; Kim, H.-R.; Hong, S.-Y. Heavy Rainfall over Korea during 1980~1990. *Korean J. Atmos. Sci.* **1998**, *1*, 32–50.
5. Sun, J.-H.; Lee, T.-Y. A Numerical Study of an Intense Quasi-Stationary Convection Band over the Korean Peninsula. *J. Meteorol. Soc. Jpn.* **2002**, *80*, 1221–1245. [CrossRef]
6. Shin, U.J.; Lee, T.Y. Origin, Evolution and Structure of Meso-α-Scale Lows Associated with Cloud Clusters and Heavy Rainfall over the Korean Peninsula. *Asia Pac. J. Atmos. Sci.* **2015**, *51*, 259–274. [CrossRef]
7. Jo, E.; Park, C.; Son, S.W.; Roh, J.W.; Lee, G.W.; Lee, Y.H. Classification of Localized Heavy Rainfall Events in South Korea. *Asia Pac. J. Atmos. Sci.* **2020**, *56*, 77–88. [CrossRef]
8. Park, H.-I.; Chung, S.-R.; Park, K.-H.; Moon, J.-I. Development of GK2A Convective Initiation Algorithm for Localized Torrential Rainfall Monitoring. *Atmosphere* **2021**, *31*, 489–510. [CrossRef]
9. Yoon, J.-H.; Min, K.-H. Characteristic Analysis of Multicell Convective System That Occurred on 6 August 2013 over the Korean Peninsula. *Atmosphere* **2016**, *26*, 321–336. [CrossRef]
10. Kim, H.-J. Statistical Analysis of Recent Lightning and the Prediction Using Rawinsonde Data Over South Korea. Master's Thesis, Kongju National University, Gongju, Republic of Korea, 2008.
11. Eom, H.-S.; Suh, M.-S. Statistical Characteristics of Recent Lightning Occurred Over South Korea. *J. Korean Earth Sci. Soc.* **2009**, *30*, 210–222. [CrossRef]
12. Chakraborty, R.; Chakraborty, A.; Basha, G.; Ratnam, M.V. Lightning Occurrences and Intensity over the Indian Region: Long-Term Trends and Future Projections. *Atmos. Chem. Phys.* **2021**, *21*, 11161–11177. [CrossRef]
13. Simon, T.; Mayr, G.J.; Morgenstern, D.; Umlauf, N.; Zeileis, A. Amplification of Annual and Diurnal Cycles of Alpine Lightning. *Clim. Dyn.* **2023**, *61*, 4125–4137. [CrossRef]
14. Pérez-Invernón, F.J.; Gordillo-Vázquez, F.J.; Huntrieser, H.; Jöckel, P. Variation of Lightning-Ignited Wildfire Patterns under Climate Change. *Nat. Commun.* **2023**, *14*, 739. [CrossRef]
15. Mäkelä, A.; Saltikoff, E.; Julkunen, J.; Juga, I.; Gregow, E.; Niemelä, S. Cold-Season Thunderstorms in Finland and Their Effect on Aviation Safety. *Bull. Am. Meteorol. Soc.* **2013**, *94*, 847–858. [CrossRef]
16. Rodríguez-Pérez, J.R.; Ordóñez, C.; Roca-Pardiñas, J.; Vecín-Arias, D.; Castedo-Dorado, F. Evaluating Lightning-Caused Fire Occurrence Using Spatial Generalized Additive Models: A Case Study in Central Spain. *Risk Anal.* **2020**, *4*, 1418–1437. [CrossRef] [PubMed]
17. Kim, H.-I.; Choi, E.-H.; Suh, S.-H.; Seo, S.-G. A Study on the Characteristics of Lightning Detection over the Naro Space Center. *J. Environ. Sci. Int.* **2022**, *31*, 543–553. [CrossRef]
18. Myoung, J.-S.; Suh, M.-S. Characteristics by the Cloud-to-Ground Lightning Polarity Occurred Over South Korea. *J. Korean Earth Sci. Soc.* **2010**, *31*, 335–347. [CrossRef]
19. Koshak, W.J.; Cummins, K.L.; Buechler, D.E.; Vant-Hull, B.; Blakeslee, R.J.; Williams, E.R.; Peterson, H.S. Variability of CONUS Lightning in 2003–2012 and Associated Impacts. *J. Appl. Meteorol. Climatol.* **2015**, *54*, 15–41. [CrossRef]
20. Unnikrishnan, C.K.; Pawar, S.; Gopalakrishnan, V. Satellite-Observed Lightning Hotspots in India and Lightning Variability over Tropical South India. *Adv. Space Res.* **2021**, *68*, 1690–1705. [CrossRef]
21. Mondal, U.; Kumar Panda, S.; Das, S.; Sharma, D.; Panda, S.K. Spatio-Temporal Variability of Lightning Climatology and Its Association with Thunderstorm Indices Over India. *Theor. Appl. Climatol.* **2022**, *149*, 273–289. [CrossRef]
22. Eom, H.-S.; Suh, M.-S. Analysis of Stability Indexes for Lightning by Using Upper Air Observation Data Over South Korea. *Atmosphere* **2010**, *20*, 467–482.
23. Sfică, L.; Apostol, L.; Istrate, V.; Lesenciuc, D.; Necula, M.F. Instability Indices as Predictors of Atmospheric Lightning—Moldova Region Study Case. In Proceedings of the 15th International Multidisciplinary Scientific GeoConference SGEM 2015, Conference Proceedings—Hydrology and Water Resources, Flamingo Grand Congress Center, Albena, Bulgaria, 16–25 June 2015. [CrossRef]
24. Bang, Y.S. The Statistical Analysis of Lightning Observed by LINET and the Characteristics of Polarimetric Radar Variables in Thunder Clouds. Ph.D. Thesis, Pukyong National University, Busan, Republic of Korea, 2023.
25. Baek, S.-K.; Choi, Y.-J.; Chung, C.-Y.; Cho, C.-H. The Characteristics and Predictability of Convective System Based on GOES-9 Observations during the Summer of 2004 over East Asia. *Atmosphere* **2006**, *16*, 225–234.
26. Machado, L.A.T.; Lima, W.F.A.; Pinto, O.; Morales, C.A. Relationship between Cloud-to-Ground Discharge and Penetrative Clouds: A Multi-Channel Satellite Application. *Atmos. Res.* **2009**, *93*, 304–309. [CrossRef]
27. Lee, Y.-J.; Suh, M.-S.; Eom, H.-S.; Seo, E.-K. Characteristics of Brightness Temperature of Geostationary Satellite on Lightning Events during Summer over South Korea. *J. Korean Earth Sci. Soc.* **2009**, *30*, 744–758. [CrossRef]
28. Lee, J.G.; Min, K.H.; Park, H.; Kim, Y.; Chung, C.Y.; Chang, E.C. Improvement of the Rapid-Development Thunderstorm (RDT) Algorithm for Use with the GK2A Satellite. *Asia Pac. J. Atmos. Sci.* **2020**, *56*, 307–319. [CrossRef]
29. Yu, H.Y.; Suh, M.S.; Ryu, S.O. Improvement of Thunderstorm Detection Method Using GK2A/AMI, RADAR, Lightning, and Numerical Model Data. *Korean J. Remote Sens.* **2021**, *37*, 41–55. [CrossRef]

30. Mikuš, P.; Strelec Mahović, N. Satellite-Based Overshooting Top Detection Methods and an Analysis of Correlated Weather Conditions. *Atmos. Res.* **2013**, *123*, 268–280. [CrossRef]
31. Khlopenkov, K.V.; Bedka, K.M.; Cooney, J.W.; Itterly, K. Recent Advances in Detection of Overshooting Cloud Tops from Longwave Infrared Satellite Imagery. *J. Geophys. Res.* **2021**, *126*, e2020JD034359. [CrossRef]
32. Han, H.; Lee, S.; Im, J.; Kim, M.; Lee, M.I.; Ahn, M.H.; Chung, S.R. Detection of Convective Initiation Using Meteorological Imager Onboard Communication, Ocean, and Meteorological Satellite Based on Machine Learning Approaches. *Remote Sens.* **2015**, *7*, 9184–9204. [CrossRef]
33. Cintineo, J.L.; Pavolonis, M.J.; Sieglaff, J.M.; Wimmers, A.; Brunner, J.; Bellon, W. A Deep-Learning Model for Automated Detection of Intense Midlatitude Convection Using Geostationary Satellite Images. *Weather Forecast.* **2020**, *35*, 2567–2588. [CrossRef]
34. Cintineo, J.L.; Pavolonis, M.J.; Sieglaff, J.M. ProbSevere LightningCast: A Deep-Learning Model for Satellite-Based Lightning Nowcasting. *Weather Forecast.* **2022**, *37*, 1239–1257. [CrossRef]
35. Cross, T.; Smit, J.R.; Schumann, C.; Warner, T.A.; Hunt, H.G.P. Deep Learning for High-Speed Lightning Footage—A Semantic Segmentation Network Comparison. *Atmosphere* **2024**, *15*, 873. [CrossRef]
36. Lesejane, W.; Hunt, H.G.P.; Schumann, C.; Ajoodha, R. Can Bayesian Networks Improve Ground-Strike Point Classification? *Atmosphere* **2024**, *15*, 776. [CrossRef]
37. Goodman, S.J.; Blakeslee, R.J.; Koshak, W.J.; Mach, D.; Bailey, J.; Buechler, D.; Carey, L.; Schultz, C.; Bateman, M.; McCaul, E.; et al. The GOES-R Geostationary Lightning Mapper (GLM). *Atmos. Res.* **2013**, *125–126*, 34–49. [CrossRef]
38. Bateman, M.; Mach, D.; Stock, M. Further Investigation into Detection Efficiency and False Alarm Rate for the Geostationary Lightning Mappers Aboard GOES-16 and GOES-17. *Earth Space Sci.* **2021**, *8*, e2020EA001237. [CrossRef]
39. NMSC. Information of GK2A. Available online: https://nmsc.kma.go.kr/enhome/html/base/cmm/selectPage.do?page=satellite.gk2a.intro (accessed on 5 July 2024).
40. De Coning, E. Optimizing Satellite-Based Precipitation Estimation for Nowcasting of Rainfall and Flash Flood Events over the South African Domain. *Remote Sens.* **2013**, *5*, 5702–5724. [CrossRef]
41. Zhang, X.; Yin, Y.; Kukulies, J.; Li, Y.; Kuang, X.; He, C.; Lapierre, J.L.; Jiang, D.; Chen, J. Revisiting Lightning Activity and Parameterization Using Geostationary Satellite Observations. *Remote Sens.* **2021**, *13*, 3866. [CrossRef]
42. Geostationary Lightning Mapper (GLM). Available online: https://ghrc.nsstc.nasa.gov/lightning/overview_glm.html (accessed on 15 September 2024).
43. Betz, H.D.; Schmidt, K.; Laroche, P.; Blanchet, P.; Oettinger, W.P.; Defer, E.; Dziewit, Z.; Konarski, J. LINET-An International Lightning Detection Network in Europe. *Atmos. Res.* **2009**, *91*, 564–573. [CrossRef]
44. About WWLLN. Available online: https://wwlln.net/ (accessed on 17 September 2024).
45. STARNET System Overview. Available online: https://raiosonline.iag.usp.br/sistema.php (accessed on 17 September 2024).
46. Korea Meteorological Administration. *Lightning Annual Report*; Korea Meteorological Administration: Seoul, Republic of Korea, 2020; ISSN 2733-483X. Available online: https://www.kma.go.kr/kma/archive/pub.jsp?field1=grp&text1=lgt_yearly (accessed on 20 June 2024).
47. Validation Report of the Convection Product Processors of the NWC/GEO. Available online: https://www.nwcsaf.org/Downloads/GEO/2018/Documents/Scientific_Docs/NWC-CDOP3-GEO-MF-PI-SCI-VR-Convection_v1.0.pdf (accessed on 17 September 2024).
48. Kunz, M. The Skill of Convective Parameters and Indices to Predict Isolated and Severe Thunderstorms. *Nat. Hazards Earth Syst. Sci.* **2007**, *7*, 327–342. [CrossRef]
49. Scofield, R.A.; Kuligowski, R.J.; Qiu, S. Combining lightning with satellite data for analysis and prediction. In Proceedings of the Conference on Meteorological Applications of Lightning Data, San Diego, CA, USA, 9–13 January 2005.
50. Schmetz, J.; Tjemkes, S.A.; Gube, M.; Van De Berg, L. Monitoring Deep Convection and Convective Overshooting with METEOSAT. *Adv. Space Res.* **1997**, *19*, 433–441. [CrossRef]
51. Ackerman, S.A.; Smith, W.L.; Revercomb, H.E.; Spinhirne, J.D. The 27–28 October 1986 FIRE IFO Cirrus Case Study: Spectral Properties of Cirrus Clouds in the 8–12 μm Window. *Mon. Weather Rev.* **1990**, *118*, 2377–2388. [CrossRef]
52. Ushio, T.; Heckman, S.J.; Boccippio, D.J.; Christian, H.J.; Kawasaki, Z.I. A Survey of Thunderstorm Flash Rates Compared to Cloud Top Height Using TRMM Satellite Data. *J. Geophys. Res.* **2001**, *106*, 24089–24095. [CrossRef]
53. Lee, Y.; Kummerow, C.D.; Ebert-Uphoff, I. Applying Machine Learning Methods to Detect Convection Using Geostationary Operational Environmental Satellite-16 (GOES-16) Advanced Baseline Imager (ABI) Data. *Atmos. Meas. Tech.* **2021**, *14*, 2699–2716. [CrossRef]
54. Charles, A.D., III; Davies-Jones, R.; David, L.K. On Summary Measures of Skill in Rare Event Forecasting Based on Contingency Tables. *Weather Forecast.* **1990**, *5*, 576–585.
55. Orlanski, I. A Rational Subdivision of Scales for Atmospheric Processes. Bull. *Am. Meteorol. Soc.* **1975**, *56*, 527–530.
56. Ávila, E.E.; Bürgesser, R.E.; Castellano, N.E.; Collier, A.B.; Compagnucci, R.H.; Hughes, A.R.W. Correlations between Deep Convection and Lightning Activity on a Global Scale. *J. Atmos. Sol. Terr. Phys.* **2010**, *72*, 1114–1121. [CrossRef]
57. Buiat, M.; Porcù, F.; Dietrich, S. Observing Relationships between Lightning and Cloud Profiles by Means of a Satellite-Borne Cloud Radar. *Atmos. Meas. Tech.* **2017**, *10*, 221–230. [CrossRef]
58. Kim, S.; Song, H.-J.; Lee, H.; Forecast, A.W. Mesoscale Features and Forecasting Guidance of Heavy Rain Types over the Korean Peninsula. *Atomosphere* **2019**, *29*, 463–480. [CrossRef]

59. Solimine, S.L.; Zhou, L.; Raghavendra, A.; Cai, Y. Relationships between Intense Convection, Lightning, and Rainfall over the Interior Congo Basin Using TRMM Data. *Atmos. Res.* **2022**, *273*, 106164. [CrossRef]
60. Medici, G.; Cummins, K.L.; Cecil, D.J.; Koshak, W.J.; Rudlosky, S.D. The Intracloud Lightning Fraction in the Contiguous United States. *Mon. Weather Rev.* **2017**, *145*, 4481–4499. [CrossRef]
61. Thiel, K.C.; Calhoun, K.M.; Reinhart, A.E.; MacGorman, D.R. GLM and ABI Characteristics of Severe and Convective Storms. *J. Geophys. Res.* **2020**, *125*, e2020JD032858. [CrossRef]
62. Cecil, D.J.; Buechler, D.E.; Blakeslee, R.J. Gridded Lightning Climatology from TRMM-LIS and OTD: Dataset Description. *Atmos. Res.* **2014**, *135–136*, 404–414. [CrossRef]
63. Chronis, T.; Koshak, W.J. Diurnal Variation of TRMM/LIS Lightning Flash Radiances. *Bull. Am. Meteorol. Soc.* **2017**, *98*, 1453–1470. [CrossRef]
64. Peterson, M. Research Applications for the Geostationary Lightning Mapper Operational Lightning Flash Data Product. *J. Geophys. Res.* **2019**, *124*, 10205–10231. [CrossRef]
65. Liu, Y.; Wang, H.; Li, Z.; Wang, Z. A Verification of the Lightning Detection Data from FY-4A LMI as Compared with ADTD-2. *Atmos. Res.* **2021**, *248*, 105163. [CrossRef]

Disclaimer/Publisher's Note: The statements, opinions and data contained in all publications are solely those of the individual author(s) and contributor(s) and not of MDPI and/or the editor(s). MDPI and/or the editor(s) disclaim responsibility for any injury to people or property resulting from any ideas, methods, instructions or products referred to in the content.